Article

pubs.acs.org/Biomac

Squid Suckerin Biomimetic Peptides Form Amyloid-like Crystals with Robust Mechanical Properties

Shu Hui Hiew,[†] Antoni Sánchez-Ferrer,[‡] Shahrouz Amini,[†] Feng Zhou,[†] Jozef Adamcik,[‡] Paul Guerette,[†] Haibin Su,[†] Raffaele Mezzenga,*[,‡] and Ali Miserez*[,†,§]

[†]School of Materials Science and Engineering, Nanyang Technological University, Singapore 639798, Singapore

[‡]Department of Health Sciences & Technology, ETH Zurich, Zurich CH-8092, CH-8093, Switzerland

[§]School of Biological Sciences, Nanyang Technological University, Singapore 637551, Singapore

Supporting Information

ABSTRACT: We present the self-assembly of fibers formed from a peptide sequence (**A1H1**) derived from suckerin proteins of squid sucker ring teeth (SRT). SRT are protein-only biopolymers with an unconventional set of physicochemical and mechanical properties including high elastic modulus coupled with thermoplastic behavior. We have identified a conserved peptide building block from suckerins that possess the ability to assemble into materials with similar mechanical properties as the native SRT. **A1H1** displays amphiphilic characteristics and self-assembles from the bottom-up into mm-scale fibers initiated by the addition of a polar aprotic solvent. **A1H1** fibers are thermally resistant up to 239 °C, coupled with an elastic modulus of ~7.7 GPa, which can be explained by the tight packing of β-sheet-enriched crystalline building blocks as identified by wide-angle X-ray scattering (WAXS), with intersheet and interstrand distances of 5.37 and 4.38 Å, respectively. A compact packing of the peptides at their Ala-rich terminals within the fibers was confirmed from molecular dynamics simulations, and we propose a hierarchical model of fiber assembly of the mature peptide fiber.

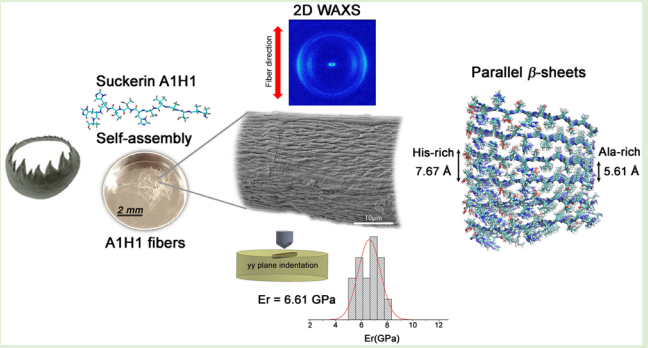

INTRODUCTION

Peptides have been studied extensively for their ability to assemble into nanoscale functional materials in various applications.[1] Designer peptides aim at rationally designing *de novo* peptide sequences based on the side-chain functionalities, while biomimetic peptides are constructed using identified sequences in natural biological protein-based structures. Sucker ring teeth (SRT) proteins (suckerins) from Humboldt squids provide a promising system for biomimicry owing to their robust mechanical properties[2,3] and their highly modular peptide building blocks. SRT are solely made of protein building blocks,[2] which were recently sequenced by combining RNA-sequencing with high-throughput proteomics.[3,4] Suckerins are constructed by modular Gly-, Ala-, and His-rich peptide motifs,[5,6] with each module playing a specific role in the structural integrity and assembly of the teeth.

Ala- (**A1**) and His-rich (**H1**) motifs in suckerins are usually flanked by Pro residues (Pro-**A1H1**-Pro) and assemble into a β-sheet rich supramolecular network, with Pro residues strongly suggested to constraint the size of β-sheets within SRT.[4] We previously found that a six amino acid long suckerin peptide (**A1**: AATAVS) was able to spontaneously form cross-β amyloidogenic short fibers in solution.[5] On the basis of this study and previous reports on the full-length suckerin-19 protein, we identified this modular and repetitive short peptide as the building block and possible seeding nucleus of β-sheet formation during the SRT self-assembly process. In parallel, although suckerin His-rich peptide motifs (**H1** and **H2**) do not self-assemble into larger fibrillar structures (such as the **A1** peptide), they initially adopted the polyproline II (PPII) conformation,[7−11] which transitioned into transient β-sheets over time, with a more pronounced transition observed at pH 7. A noteworthy observation was that **A1** peptide self-assembled into microfibers at concentrations as low as 0.5 mg/mL near neutral pH, whereas preliminary data indicated that **H1** peptide was characterized by a much higher solubility (above 50 mg/mL) in the same solvent. We thus hypothesized that **H1** mediates the formation of SRT by maintaining a high solubility of suckerins prior to supra-molecular assembly, whereas **A1** acts as a seed for β-sheet formation and fibrillization. In this work, using a reductionist approach, we aimed to test this hypothesis and to construct a robust peptide-based material designed after the modular peptide motifs of suckerins. We prepared a larger suckerin peptide comprising

Received: September 5, 2017
Revised: October 31, 2017
Published: November 7, 2017

DOI: 10.1021/acs.biomac.7b01280
Biomacromolecules 2017, 18, 4240−4248

both the Ala- and His-rich sequences (**A1H1**; peptide sequence AATAVSHTTHHA) and investigated its self-assembly behavior, structure, as well as its nanoscale mechanical properties. **A1H1** peptide sequence has an amphiphilic character, and we find that it is capable of self-assembling into mechanically robust millimeter-scale fibers owing to its unusual tight inter-β-sheet packing. Molecular dynamics (MD) simulations also suggest asymmetric packing of β-sheets where the Ala-rich domains are more tightly packed than the His-rich domains.

MATERIALS AND METHODS

Materials. Fmoc-protected amino acids, chlorotrityl chloride resins, and HATU were purchased from GL Biochem Ltd. (Shanghai, China). Piperidine was purchased from Acros Organics (Fisher Scientific Pte Ltd., Singapore), diisopropylethylamine (DIEA) was purchased from Alfa Aesar (Massachusetts, USA), and 5% picrylsulfonic acid solution, triisopropylsilane (TIPS), and trifluoroacetic acid (TFA) were purchased from Sigma-Aldrich (Singapore). All other solvents were purchased from Fisher Chemical (Singapore) and Tedia (Ohio, USA) unless otherwise specified. All of the chemical reagents and solvents from commercial sources were used without further purification. A customized glass reaction vessel was used for solid phase peptide synthesis.

Solid Phase Synthesis and Purification of Peptide A1H1. Peptide synthesis was performed from C- to N-terminal according to standard solid phase peptide synthesis (SPPS) procedures using chlorotrityl chloride resins. Resins were preswelled in a reaction vessel with dichloromethane (DCM) (30 min) prior to addition of activation cocktail (1.5 equiv Fmoc-protected amino acid and 2 equiv DIEA) for 1 h. Stringent washing (3× DCM, 3× dimethylformamide (DMF), 3× DCM) was then performed to remove unreacted reagents and side products. Capping of unreacted chloride groups was done by adding DCM, MeOH, and DIEA (85:10:5) and mixed for 1 h. Resins were then washed thoroughly with 3× DCM and 3× DMF, followed by adding deprotection solution of 20% piperidine in DMF (30 min) to remove the Fmoc protecting group on the amino acid. Stringent washing (3× DMF, 3× DCM, 3× DMF) was performed again to remove side products after filtering the resins, and a 2,4,6-Trinitrobenzene Sulfonic Acid (TNBS) colorimetric assay was performed on a few beads to check for the presence of free amine (and completion of deprotection). TNBS assay was performed by adding 2.5 μL of 5% picrylsulfonic acid solution to an aliquot of 300 μL of 10% DIEA in DMF containing the beads. Bright orange coloration of the beads was observed for successfully deprotected Fmoc-amino acid indicating the presence of free amine. Subsequent addition of amino acid residues was performed by adding coupling cocktails of 2 equiv Fmoc-protected amino acid, 1.9 equiv HATU, and 5 equiv DIEA in DMF. Between deprotection and coupling steps, stringent washing was strictly followed. Final deprotection of amino side chain protecting groups and cleavage of synthesized peptide from resin was performed by adding TFA, TIPS, and water in a V/V ratio of 9.5:0.25:0.25 for 2 h. Resins were then filtered and TFA was removed from the filtrate via rotaevaporation. Cold diethyl ether was then used to precipitate and wash the peptides to remove the side products. Peptide was desiccated and kept at −20 °C. Peptide was purified by performing minimally two rounds of reverse phase high-performance liquid chromatography (HPLC) on Agilent Infinity 1260, using an Agilent 300SB C18 column to achieve at least 95% purity, prior to use. Molecular weight of the purified peptide was verified via liquid chromatography−mass spectrometry (LC−MS) in ESI+ mode on a Thermo Finnigan LCQ Fleet MS (Massachusetts, USA).

Circular Dichroism (CD) Spectroscopy. Peptides were prepared at 5 mg/mL, and spectra were collected using a quartz cuvette with optical path length of 0.2 mm. Data acquisition was performed by AVIV 420 Circular Dichroism (New Jersey, USA) spectrometer in wavelength steps of 0.5 nm with an averaging time of 0.1 s, at 1.00 nm bandwidth and a wavelength range from 190 to 260 nm, averaging over three scans. The obtained spectra were smoothed at 10 points via adjacent-averaging method (noting to not remove any existing peaks or introduce artifacts) and plotted via OriginPro 9.1.

Dynamic Light Scattering (DLS). Peptides were dissolved in buffers of pH 4 (0.1 M acetate buffer), pH 7 (0.1 M phosphate-buffered saline), pH 8.2 (0.1 M tris-buffered saline), and in 8 M urea, at 5 mg/mL immediately prior to DLS measurements. All buffers were filtered immediately prior to measurements, and each data set was collected over a minimum of five scans of 5 s duration, with a backscatter angle of 173° on a Malvern Zetasizer Nano ZS (Worcestershire, UK).

Scanning Electron Microscopy (SEM) Imaging. Peptide fibers obtained from 95:5 (V/V) water/ACN solution were removed with tweezers and air-dried on carbon tape. Dried fibers were coated with Platinum below 5 Pa, at 20 mA for 60 s prior to imaging. Imaging was performed using JEOL JSM-FESEM 7600F (Massachusetts, USA).

Atomic Force Microscopy (AFM) Imaging. A droplet of peptide fiber solution (95:5 (V/V) water/ACN) was deposited on freshly cleaved mica, adsorbed for 2 min at room temperature, and gently dried with pressurized air. The sample was scanned on a Bruker Nanoscope VIII Multimode Scanning Force Microscope (Massachusetts, USA) covered with an acoustic hood to minimize vibrational noise. The AFM was operated in tapping mode under ambient conditions using commercial silicon nitride cantilevers. All AFM images were flattened to remove background curvature using the Nanoscope Analysis 1.5 software and no further image processing was carried out.

Nanoindentation. Peptide fibers were air-dried and embedded in epoxy. Gradual polishing of the epoxy puck was performed to obtain the cross-sections of the embedded fibers (*xx* and *yy* cross-sections) prior to nanoindentation performed with a Hysitron TI 950 Triboindenter (Minnesota, USA) and a Berkovich (cube-corner) indentation tip. The tip was calibrated with a fused quartz standard sample of $\overline{E}$ = 69.9 GPa ± 10%. Scanning probe microscopy images were first obtained prior to each set of indentation, and indentations were performed with loading forces ranging from 15−50 μN. Samples were air-dried overnight (at least 12 h) to obtain indentations for dried fibers, while the fibers were hydrated in water for at least an hour prior to and during indentations for hydrated fibers. Load−hold−unload indentation function setup was applied for all indents, with segment intervals of 5 s (load), 2 s (hold), and 5 s (unload). Loading−unloading curves indicating indents affected by substrates were discarded, and the average modulus values of each sample set were obtained from at least 15 indents.

Congo Red Birefringence Assay. Congo red staining was done on air-dried fibers removed from solution. A mixture of 80:20 V/V of ethanol/water was added with a saturating amount of NaCl and excess salt was filtered off. A saturating amount of Congo Red was added and vortexed until no more dye could be dissolved, then filtered again with a 0.2 μm filter and used immediately. Staining solution was pipetted onto the dried fibers and all fibers were ensured to be covered with the staining solution. Excess staining solution was blotted away with lint-free filter paper after 20 s, and fibers were allowed to dry at ambient temperature before being viewed under an optical microscope. Stained fibers were viewed with a Carl Ziess Axio Imager (Oberkochen, Germany) under both normal and polarized light.

Differential Scanning Calorimetry (DSC). Air-dried peptide fibers of known mass were placed into a preweighed Tzero pan and lid, and DSC measurements were performed with TA Instruments Discovery DSC (Delaware, USA) under nitrogen atmosphere with 50 mL/min flow rate. Temperature was increased at a rate of 5 °C/min from 40 to 400 °C. The obtained calorimetry curves were normalized with the sample weight, and analysis was done on TA Universal Analysis software.

Thermogravimetric Analysis (TGA). Peptide powder of known mass was placed onto a TGA sample holder, and measurements were performed on a TA Instruments TGA Q500 (Delaware, USA) equipment, under nitrogen atmosphere, with a nitrogen gas flow rate of 60 mL/min. Measurements were recorded from room temperature to 400 °C, with a temperature increase rate of 5 °C/min. Subsequent analysis was done on TA Universal Analysis software.

DOI: 10.1021/acs.biomac.7b01280
Biomacromolecules 2017, 18, 4240−4248

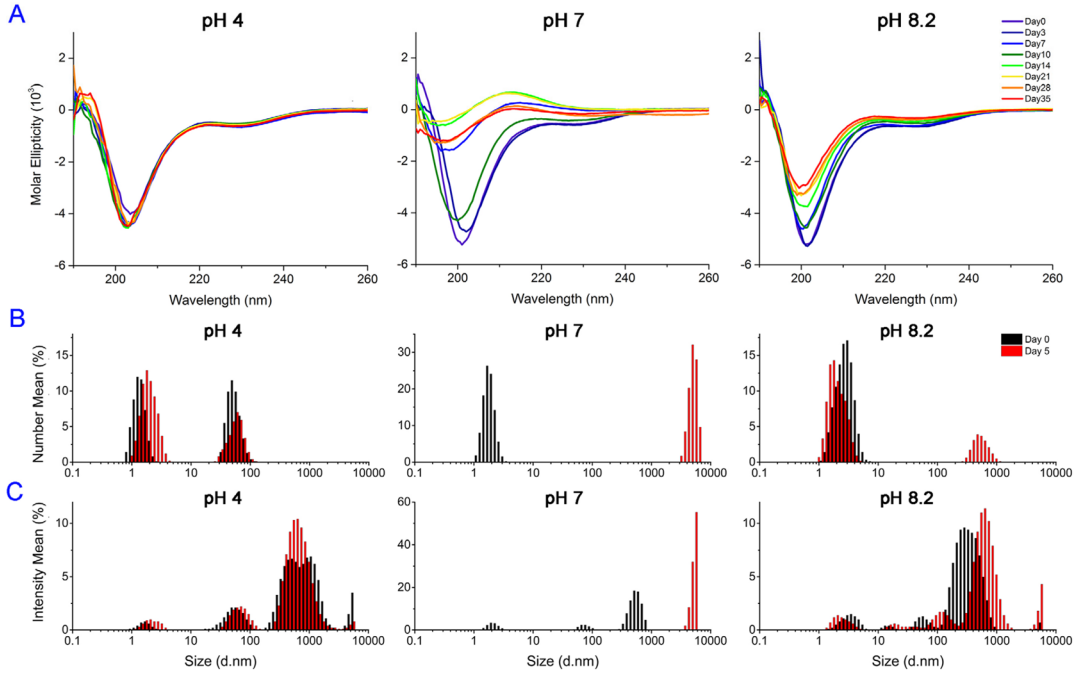

Figure 1. Time-series study of A1H1 peptide secondary structural changes and its size distribution. (A) Thirty-five-day time series CD spectra of peptide **A1H1** in aqueous buffers at room temperature. CD spectra were obtained from the 5 mg/mL peptide solutions incubated at pH 4, 7, and 8.2, respectively. DLS measurements were obtained at day 0 and day 5 to probe the size distributions of the peptide solutions, presented in (B) number mean percentage and (C) intensity mean percentage.

Wide-Angle X-ray Scattering (WAXS). WAXS experiments were performed using a Rigaku MicroMax-002+ (Tokyo, Japan) micro-focused beam (40 W, 45 kV, 0.88 mA) with the $\lambda_{CuK\alpha}$ = 0.15418 nm irradiation collimated by three pinhole collimators (0.4, 0.3, and 0.8 mm). The scattered WAXS intensity was collected in transmission mode by a two-dimensional Fujifilm BAS-MS 2025 imaging plate system (15.2 × 15.2 cm^2, 50 μm resolution). An effective scattering vector range of 1 $nm^{-1} < q < 25$ nm^{-1} was obtained, where q is the scattering wave vector defined as $q = 4\pi \sin\theta/\lambda_{CuK\alpha}$ with a scattering angle of 2θ.

Fourier-transform infrared (FTIR). FTIR spectra of A1H1 fibers were obtained using a Varian 640 FTIR spectrometer (California, USA) equipped with a Specac Diamond ATR Golden Gate single attenuated total reflection (ATR) system. Samples were scanned at room temperature over the range of 4000 to 600 cm^{-1} with a resolution of 4 cm^{-1}, averaged over 64 scans, and baseline corrected. The amide region was normalized, resolved by second-derivative analysis, and peak deconvoluted using Igor Pro 6.3.4.1 software.

FTIR spectra of A1H1 peptide in D_2O buffers were obtained using a Bruker Vertex 70 (Massachusetts, USA) spectrometer equipped with a PIKE Technologies Diamond/ZnSe ATR accessory. Samples were scanned at room temperature over the range of 4000 to 800 cm^{-1}, averaged over 280 scans. Baseline correction was performed prior to secondary derivative deconvolution of amide I region using OPUS 6.5 software.

MD Simulations. The simulations were performed by using the GROMACS package.[12] The overall temperature of the water and peptides was kept constant, coupling independently each group of molecules at 300 K with a V-rescale thermostat.[13] The pressure was coupled to a Parrinello−Rahman[14,15] barostat at 1 atm separately in every dimension. The temperature and pressure time constants of the coupling were 0.1 and 2 ps, respectively. The integration of the equations of motion was performed by using a leapfrog algorithm with a time step of 2 fs. Periodic boundary conditions were implemented in all systems. To optimize the β-sheet fiber structure and compare to the experimental crystal cell parameters, a super cell structure (6 × 6 × 2) was used to mimic the experimental conditions. A cutoff of 1 nm was implemented for the Lennard−Jones and the direct space part of the Ewald sum for Coulombic interactions. The Fourier space part of the Ewald splitting was computed by using the particle-mesh-Ewald method,[16] with a grid length of 0.16 nm on the side and a cubic spline interpolation. We used the TIP3P water model,[17] and the peptide parameters were from the CHARM force field.[18,19]

For the binding energy calculation for H_2O/ACN/peptide system, we used COMPASS force field (Condensed-phase Optimized Molecular Potentials for Atomistic Simulation Studies), developed by H. Sun[20] as built in the Forcite package.

RESULTS AND DISCUSSION

A1H1 was prepared via solid-phase peptide synthesis and purified by reversed-phase HPLC (Figure S1). The secondary structure composition of **A1H1** was investigated in aqueous solution using CD spectroscopy over a time period of 35 days, at a concentration of 5 mg/mL, and in three aqueous buffers of pH 4, 7, and 8.2 (Figure 1A). The three pH values were chosen such as to mimic the variations in microenvironment that the suckerins experience during their assembly process *in vivo*, from their production in epithelial cells to their exposure to the ocean's pH. Under these aqueous conditions, a general similar spectral signature was initially observed across the three pH levels, with two minima observed at 200−205 nm (strong) and ∼230 nm (weak).

At pH 4, no significant changes were observed over 35 days, with only a slight blue-shift of the strong minimum at 204 nm toward 202 nm and the weak negative shoulder remaining at 232 nm. At pH 8.2, the initial spectra displayed a strong minimum at 202 nm and a weak negative shoulder centered ∼230 nm. The intensity of the minima decreased over time to nearly half their initial values, concomitant with a blue-shift of 2 nm for each minimum (200 and 228 nm, respectively). Dramatic changes were observed at pH 7, where significant conformational transitions were detected during the second week. The initial spectra displayed an intense minimum at 201

DOI: 10.1021/acs.biomac.7b01280
Biomacromolecules 2017, 18, 4240−4248

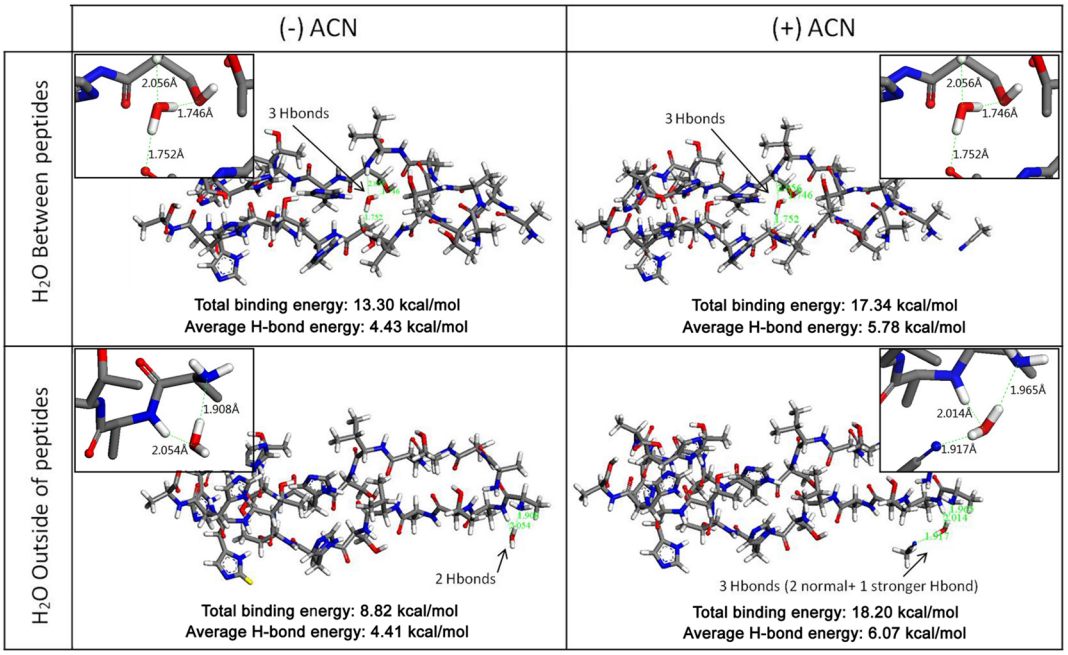

Figure 2. Comparison of hydrogen bond (H-bond) energies in the absence (−) and presence (+) of ACN. H-bond energies of water molecules between and outside of the cavity of two peptide units were obtained from MD simulations.

nm, which decreased over time and gradually blue-shifted to 197 nm. In addition, the initial weak negative shoulder at 228 nm disappeared, whereas a slight maximum appeared at 213 nm over time. The overall decrease in intensity is attributed to hypochromism of the optical transitions of the peptides' amide bonds (hence a lowered extinction coefficient),[21] which is likely due to the ordered arrangement of chromophores resulting from their self-assembly into oligomers in solution during the incubation period. No larger structures were observable with the naked eye or by optical microscopy during this period.

The spectra obtained at all three pH values were reminiscent to those of random coiled, polyproline II, or β-sheet-rich structures.[22] With previous studies pointing toward the high β-sheet propensity of the **A1** and **H1** sequences, spectral fitting was performed using the BeStSel program (Figure S2A),[22] which was designed for deconvoluting CD spectra of β-sheet-rich proteins and peptides. Deconvolution results indicated and **A1H1** formed mainly β-sheets (ca. 40%) at all three pH values as shown in Figure S2B, although we note that deconvolution results at pH 7 are considered less reliable due to the poorer spectral fitting that resulted from the weak spectral intensity at this pH. In support of the CD spectroscopy results, attenuated total reflection fourier transform infrared (ATR FTIR) spectra of the peptide solutions in their respective D_2O buffers indicated a high β-sheet content (Figure S3). Secondary derivative deconvolution of their amide I peaks between 1700 and 1600 cm^{-1} yielded a semiquantitative estimate of >65% β-sheet secondary structure.

To further probe the self-assembly behavior of these amphiphilic peptides, DLS measurements were conducted on **A1H1** peptide solutions on day 0 and after 5 days of incubation, as shown in Figure 1B and C. DLS is an advantageous technique to observe both abundant monomers as well as minute populations of larger oligomer assemblies.[23−25] **A1H1** peptides exhibited population distributions characteristic of amyloid peptides, with polydisperse populations of oligomers that strongly depended on pH. At pH 4, no changes were observed in size distribution over the incubation period, and most of the peptide solution consisted mainly of two size groups, namely the monomeric peptide and ∼50 nm oligomers. The presence of larger sized oligomers (>1 μm) was only sparingly detected (intensity mean). At pH 8.2, slight changes were observed. The peptide solution mostly consisted of peptide monomers with some presence of larger sized oligomers (ca. 50 nm and ca. 300 nm) on day 0. On day 5, a larger (ca. 500 nm) population of oligomers appeared with an overall shift in oligomer size distribution to larger sizes of ∼100 nm, 600 nm, and >5 μm (intensity mean). The most drastic changes were observed at pH 7, where the majority of the peptides were initially monomeric with only minute presence of larger sized oligomers (ca. 80 nm and ca. 500 nm). At day 5, no monomers were detected as the peptides assembled into μm-sized oligomers. The self-assembly behavior inferred from DLS thus parallels the CD results of the peptide at different pH levels, with the strongest changes observed at pH 7.

We suggest that at pH 4, the peptide remained highly stable with the same conformation over 35 days of incubation, most likely because His residues are protonated (pK_a = 6.04) and create strong electrostatic repulsion between neighboring peptides, resulting in a high stability in solution. At pH 7, a significant fraction of His residues are deprotonated (ca. 90%), allowing the peptides to come into closer proximity initially via electrostatic attraction of their terminal charges. Subsequently, hydrophobic and hydrogen bonding interactions led to assembly of interpeptide β-sheets. Similarly, at pH 8.2, His residues become almost fully deprotonated and hence able to interact and assemble into ordered β-sheet structures (Figure 1), as evidenced from the gradual reduction in CD molar ellipticity intensity due to hypochromism and DLS size distribution changes. In our previous study, **A1** peptide spontaneously aggregated into β-rich structures with a low solubility, while **H1** peptide alone remained soluble in aqueous conditions. In the present situation, fusing both peptides led to a much higher solubility combined with β-sheet propensity,

DOI: 10.1021/acs.biomac.7b01280
Biomacromolecules 2017, 18, 4240−4248

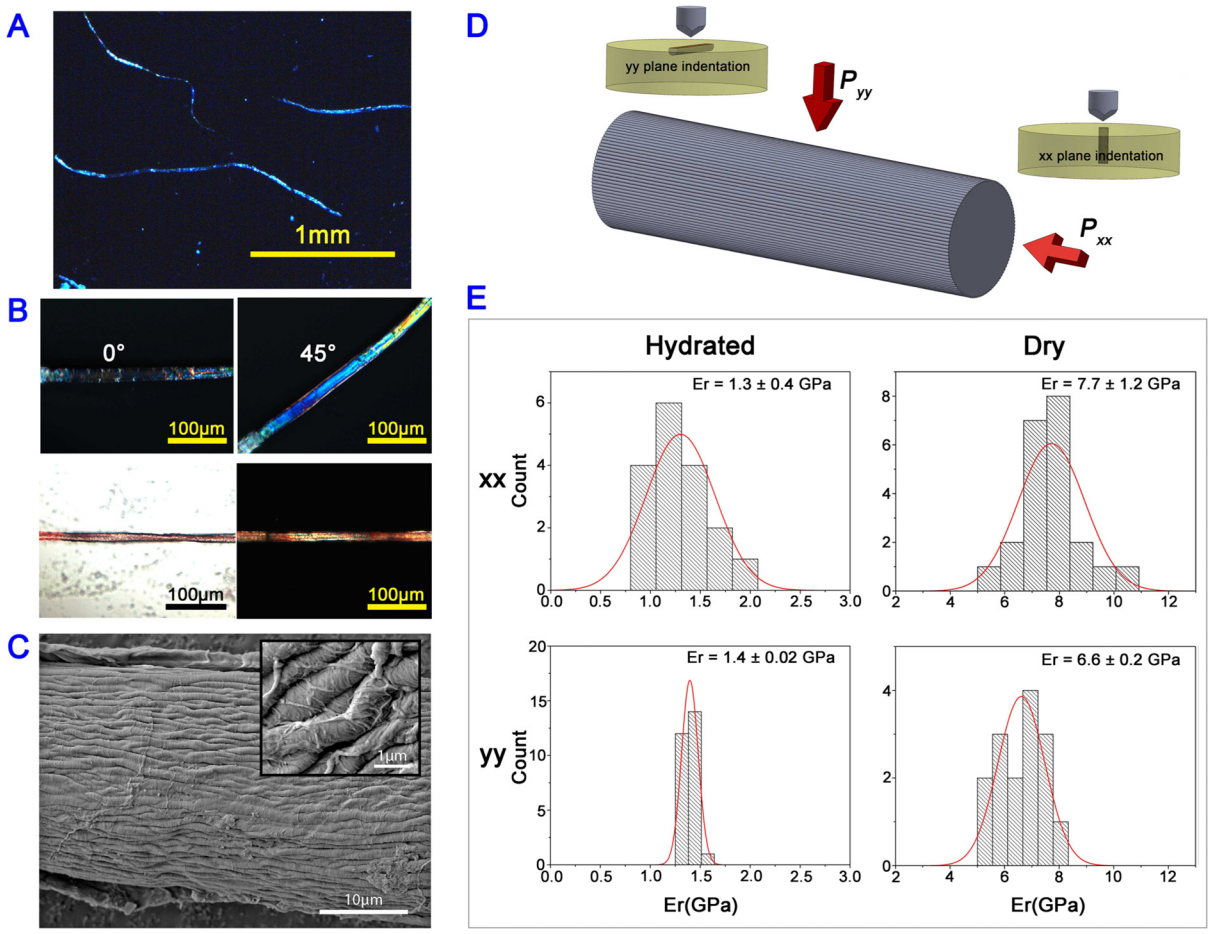

Figure 3. Characterization of self-assembled **A1H1** peptide fibers. (A) Fibers observed under polarized light optical microscopy; (B) at 0° and 45° (top) and after Congo red staining (bottom) under normal light and polarized light microscopy. (C) SEM image of a fiber, with inset showing a magnified view. (D) Illustration of nanoindentation measurements performed in two orthogonal directions on **A1H1** fibers embedded in epoxy resin. (E) Young's modulus (reduced modulus, E_r) values of the fibers obtained from nanoindentation under hydrated and dry conditions.

indicating that larger objects may assemble by increasing the solubility of the **A1H1** peptide in aqueous conditions.

To induce self-assembly into larger structures from the peptide solution, different solvent mixtures were investigated with the goal to destabilize solvent−peptide interactions and to trigger instead peptide−peptide interactions.[26−28] Long fibers of up to a few millimeters in length were quickly formed by dissolving lyophilized **A1H1** peptides in a mixture 95:5 V/V of pure water and acetonitrile (ACN) (water/ACN). The fibers were observed starting from a high peptide concentration above 50 mg/mL. The **A1H1** peptide was also found to be readily soluble up to 800 mg/mL in pure water. On the other hand, neither the same solvent mixture condition for the shorter **A1** peptide nor the increased **A1H1** peptide concentration in the aqueous buffer solutions led to the formation of large fibers. As an aprotic polar solvent, ACN can only form hydrogen bonds with protic molecules. Thus, a plausible mechanism of assembly is that ACN destabilizes the water/peptide network by competing with the peptide for hydrogen bonds with water molecules, thereby driving the latter out of the network. In turn, adjacent **A1H1** peptides come in closer proximity and quickly initiate interpeptide β-sheet formation. To substantiate this hypothesis, we performed MD simulations on the peptides in the absence and presence of ACN molecules (Figure 2). In the absence of ACN, the MD results indicated that a single water molecule preferably resides between peptides to form hydrogen bonds with the peptides, achieving a total binding energy of 13.30 kcal/mol. In contrast, the presence of ACN resulted in the single water molecule to preferably remain outside of the peptide core, which instead forms hydrogen bonds with ACN molecules with a higher total binding energy of 18.20 kcal/mol. These simulations strongly suggest that in the presence of ACN, water desolvation from the peptides is energetically favorable, therefore triggering peptide−peptide interactions and the corresponding self-assembly.

Peptide fibers formed in the presence of ACN exhibited birefringent properties (Figure 3A,B top panels), indicative of an anisotropic arrangement of the peptides in the mature fibers. When the fibers were stained with Congo red dye and viewed under polarized light (Figure 3B, bottom panels), they appeared apple-green in various locations, indicative of an amyloid-like structure.[29] SEM imaging revealed that the fibers were made up of hundreds of smaller fibers (ca. 1 μm diameter) bundled together and arranged parallel to the main fiber axis (Figure 3C). Nanoindentation was performed on the fibers, which were prepared by fixing them in epoxy resin overnight prior to polishing to obtain flat cross-sections (sample preparation described in Materials and Methods). To observe possible anisotropic behavior, indents were performed in both *xx* and *yy* directions (Figures 3D and S4) with a cube-corner tip geometry. Indentation results are shown in Figure 3E (characteristic loading/unloading curves are shown in Figure

DOI: 10.1021/acs.biomac.7b01280
Biomacromolecules 2017, 18, 4240−4248

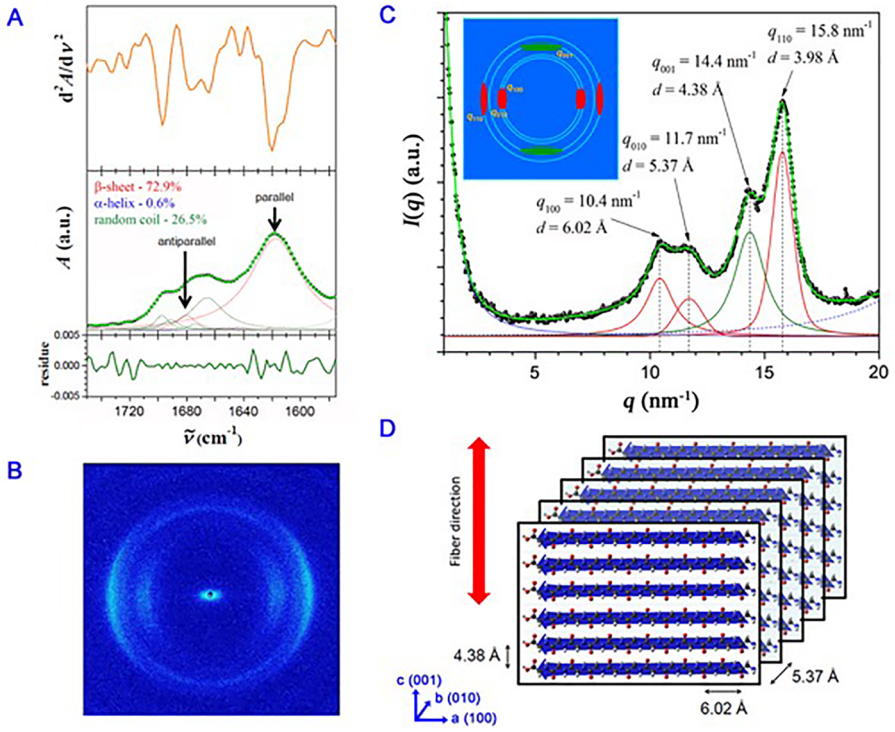

Figure 4. Characterization of peptide fibers via FTIR and WAXS. (A) Second derivative (top) of FTIR spectrum (middle) obtained from dry **A1H1** fibers. Residual difference of fitted spectra is shown at the bottom panel. (B) 2D WAXS pattern of dry **A1H1** fibers, with (C) 360°-averaged radial integration. (D) Proposed parallel β-sheet crystalline structure with assigned dimensions of the crystal inferred from the WAXS spectra.

S5). Under hydrated conditions, the modulus in the *xx* and *yy* direction was 1.3 ± 0.4 GPa and 1.4 ± 0.02 GPa, respectively. Under dried conditions, the modulus was 7.7 ± 1.2 GPa in the *xx* direction and 6.6 ± 0.2 GPa in the *yy* direction.

The **A1H1** fibers exhibited moduli values that were comparable to those previously reported for native SRT, which ranged from 2.75−1.75 GPa (tooth periphery to core) under hydrated conditions and 7.5−4.5 GPa under dry conditions.[2,3] The similar moduli obtained from probing the fibers in both *xx* and *yy* directions indicate isotropic properties of the fibers. Nanoindentation measurements were also performed on microfibers formed by **A1** peptide (Figure S6), and an average modulus of 6.9 ± 1.2 GPa (*yy* direction) was obtained under dry conditions. Hence, increasing the peptide building block length from 6 to 12 residues did not affect the mechanical property of the fibers, despite the fact that **A1H1** fibers are ∼200-times the length of the **A1** peptide fibers. These results support our hypothesis that the role of **H1** sequence is to maintain a high solubility of the proteins in solution for higher order self-assembly, whereas **A1** peptide drives self-assembly by β-sheet-induced fibrillization.

A melting temperature of ∼240 °C was recorded for **A1H1** fibers (Figure S7A) by DSC, whereas a degradation temperature of 224 °C was obtained by TGA technique for the precursor lyophilized **A1H1** powder (Figure S7B), close to that reported (220 °C) by Latza et al.[30] for native SRT, which was previously attributed to the melting of β-sheets. These results suggest that the melting temperature obtained for the **A1H1** fibers is associated with the collapse of hydrogen bonds stabilizing the β-sheets and the melting of β-strands as well as the disruption of van der Waals and hydrophobic forces within the fibers. FTIR spectroscopy of dehydrated **A1H1** fibers indicated a high β-sheet content of 72.9% after peak deconvolution and semiquantitative estimate integration of its distinct amide I peak between 1700 and 1600 cm^{-1} (Figure 4A). The deconvoluted amide I band also revealed a strong band at 1620 cm^{-1}, which is generally attributed to a parallel conformation of β-sheets.[31,32]

To better understand the structure of **A1H1** peptide fiber, we conducted WAXS measurements, and the 2D scattering pattern is shown in Figure 4B. Two equatorial reflections were observed, a sharp one and a broader one consisting of two fainter peaks, as well as one weaker meridional reflection. Radial integration (Figure 4C) resulted in *d*-spacing values for these reflections of 3.98 Å (sharp equatorial reflection), 5.37 and 6.02 Å (weaker equatorial reflections), and 4.38 Å (meridional reflection). A *d*-value of 4.38 Å matches well with the interstrand spacing of β-sheets, indicating the presence of β-strands oriented perpendicular to the fiber axis (Figure 4D), which is reminiscent of cross-β structures of amyloids.[33] Assigning the fiber axis to the (001) direction (q_{001} = 14.4 nm^{-1}), the WAXS pattern can be rationalized by considering that the β-sheets self-assemble with the sheets oriented parallel to the fiber axis, as shown in Figure 4D. The corresponding crystalline structure is the one of a monoclinic crystal of lattice parameters a = 6.02 Å, b = 5.37 Å, c = 4.38 Å, and γ = 89.3°, with a cell volume of 0.142 nm^3 and domain size of ∼77 nm^3. In this model, the (100) reflection (q_{100} = 10.4 nm^{-1}) corresponds to the strand direction with 6.02 Å the distance between adjacent carbonyl groups (i + 2), the (010) reflection (q_{010} = 11.7 nm^{-1}) to the inter-β-sheet distance of 5.37 Å, and the (110) reflection (q_{110} = 15.8 nm^{-1}) to the plane whose distance is 3.98 Å. We note that such an intersheet distance is smaller than the ones observed in typical parallel and antiparallel β-sheet crystals.[33] However, the spacing coincides with β-sheet dimensions measured for Ala-rich peptide fibers,[34]

DOI: 10.1021/acs.biomac.7b01280
Biomacromolecules 2017, 18, 4240−4248

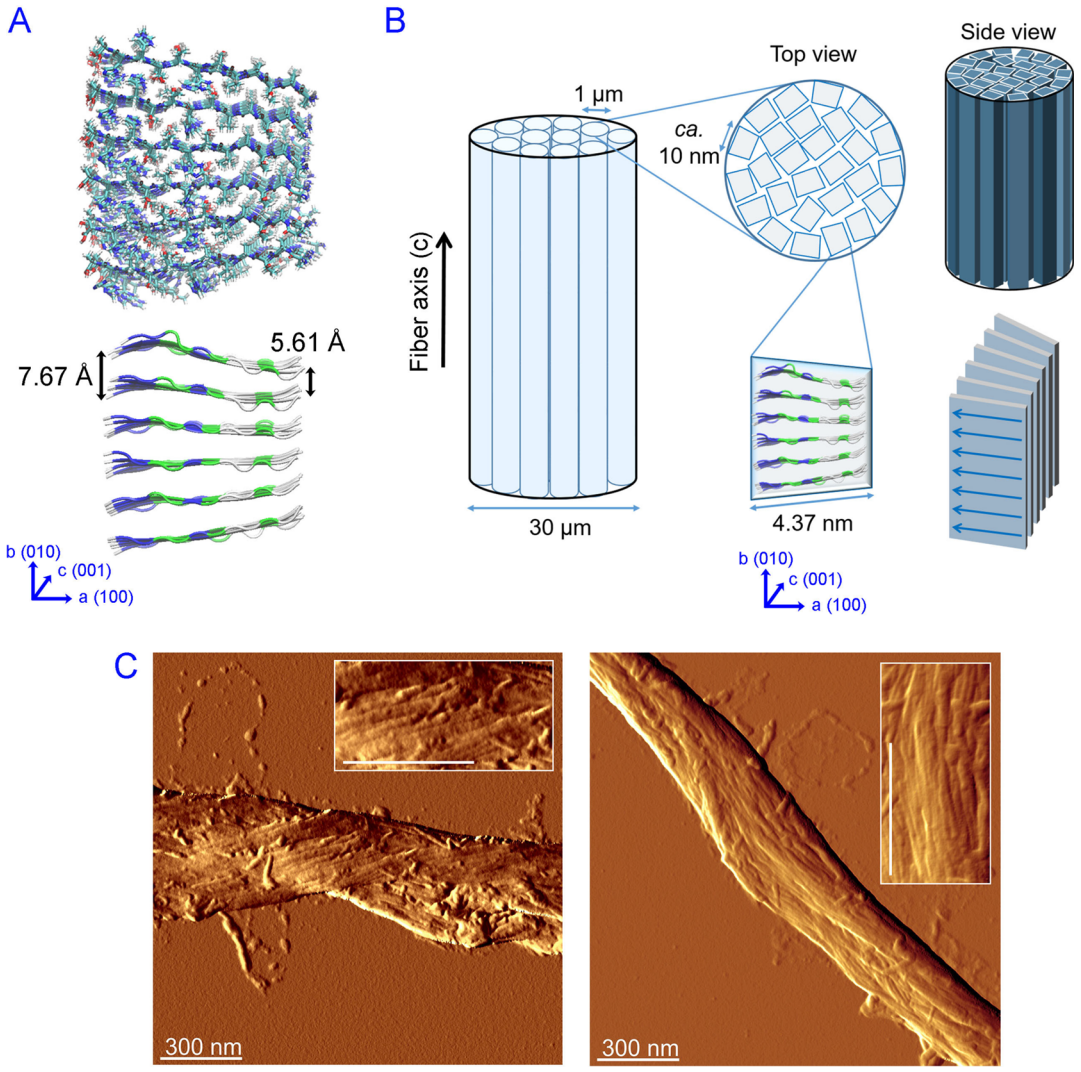

Figure 5. MD simulations of **A1H1** peptides assembly and a schematic representation of the proposed fiber model. (A) MD simulation of **A1H1** peptides in a parallel assembly with an Ala-rich end (top) and the simplified ribbon model (bottom) illustrating the difference between the intersheet distance of Ala-rich domains and the distance of adjacent His-rich domains in the (010) direction. (B) Proposed model of a single **A1H1** peptide fiber, with magnified illustrations of the nanoscale structure from top and side views. (C) AFM phase images of **A1H1** peptide fiber supporting the proposed fiber model displayed in panel B.

where intersheet distances of 5.3−5.5 Å were reported, and such shorter distances have previously been attributed to efficient packing of small Ala residues,[35,36] resulting in more compact structures with shorter hydrogen bonds.[34] It is thus reasonable to attribute the tighter packing measured by WAXS to the presence of Ala-rich domains in our **A1H1** peptide. Furthermore, the tighter molecular packing may also explain the high melting temperature of the **A1H1** fibers and their elevated mechanical properties.

To further test this hypothesis, we conducted MD simulations of the **A1H1** peptide with unconstrained boundary conditions and a parallel conformation of the β-strands. We found a significant difference between the intersheet distance of Ala-rich domains and the distance between His-rich domains in the (010) direction, with values of 5.61 and 7.67 Å, respectively (Figure 5A). Antiparallel conformation was also simulated as a control (Figure S8), and a uniform intersheet distance of 8.05 Å was calculated. Owing to the small Ala residues, the packing of the β-sheets was thus predicted to be tighter in the Ala-rich terminal of parallel conformation, which supports the WAXS data. His-rich domains, on the other hand, were less compacted due to the larger steric hindrance of the imidazole side chains. Combining the MD simulations with the experimental data, a plausible assembly of the amphiphilic **A1H1** peptide is suggested, as shown in Figure 5B. The main fiber is proposed to be constructed by smaller micron-sized fibers aligned parallel to the main fiber axis (Figure 3C), with crystalline nanoscale units constructed by **A1H1** peptides arranged in a parallel β-sheet conformation (Figures 4D and 5A). AFM phase images of **A1H1** peptide fiber displayed in Figure 5C confirmed that smaller micron-sized fibers were made of nanometer-sized fibers, supporting the proposed hierarchical fiber model sketched in Figure 5B. The stacking of these protofibrils form trapezoid-like cross-section with a more compact hydrophobic Ala-rich end, and are randomly oriented within the micron-sized fibers (Figure 5B). Peptide amphiphile fiber self-assembly is usually driven by the hydrophobic tail, and these hydrophobic or aliphatic chains tend to be buried in the fiber core, whereas the hydrophilic groups are exposed on the surface.[37−44] Since WAXS patterns indicated β-sheet dimensions

DOI: 10.1021/acs.biomac.7b01280
Biomacromolecules 2017, 18, 4240−4248

similar to those predicted from the Ala-rich domains by MD simulations, these domains are postulated to drive self-assembly by forming β-sheets that are oriented parallel to the fiber axis. On the other hand, the His-rich domains further from the hydrophobic Ala-rich segments are not believed to play a key role in self-assembly[37] and may ultimately not adopt β-sheet secondary structure.

CONCLUSION

Squid SRT are entirely built from the suckerin protein family, a block copolymer-like protein biopolymer that self-assembles into a semicrystalline network with nanoscale β-sheets embedded within an amorphous matrix. We have shown that the Ala- and His-rich peptide **A1H1**, one of the most abundant repetitive peptide motifs of the suckerin protein family, can self-assemble into large fibrillar structures. The His-rich domains help to maintain the high solubility of the **A1H1** peptides, whereas the Ala-rich domains provide the seed for subsequent β-sheet driven assembly. Self-assembly and large-scale fibrillization are triggered by disturbing the peptide/water H-bonding network of the peptide solution upon addition of an aprotic polar solvent that traps water molecules, thus driving H-bonding interactions between the peptide units. Because of its amphiphilic nature, **A1H1** self-assembles into amyloid-like fibrous crystals, with MD simulations suggesting more compact β-sheets in the Ala-rich domains as compared to the His-rich domains. The β-sheet enriched fibers lead to mechanical properties that match native SRT as well as a high temperature stability, which is attributed to the tightly packed β-sheet arrangement of the peptide sequence. Overall, this study provides molecular-scale biomimetic lessons inspired by squid suckerin modular peptides for the rational design of mechanically robust peptide-based materials.

ASSOCIATED CONTENT

Supporting Information

The Supporting Information is available free of charge on the ACS Publications website at DOI: 10.1021/acs.biomac.7b01280.

Experimental figures, deconvolution and characterization data (PDF)

AUTHOR INFORMATION

Corresponding Authors

*E-mail: ali.miserez@ntu.edu.sg.
*E-mail: raffaele.mezzenga@hest.ethz.ch.

ORCID

Haibin Su: 0000-0001-9760-6567
Raffaele Mezzenga: 0000-0002-5739-2610
Ali Miserez: 0000-0003-0864-8170

Notes

The authors declare no competing financial interest.

ACKNOWLEDGMENTS

This research was supported by the Singapore Ministry of Education (MOE) through an Academic Research Fund (AcRF) Tier 1 grant (# MOE2015-T1-002-064) and an AcRF Tier 2 grant (# MOE2015-T2-1-062). We would like to acknowledge the Facility for Analysis, Characterization, Testing and Simulation (FACTS), Nanyang Technological University, Singapore, for use of their electron microscopy facilities.

REFERENCES

(1) Aleman, C.; Bianco, A.; Venanzi, M. *Peptide Materials: From Nanostructures to Applications*; Wiley, 2013.
(2) Miserez, A.; Weaver, J. C.; Pedersen, P. B.; Schneeberk, T.; Hanlon, R. T.; Kisailus, D.; Birkedal, H. Microstructural and Biochemical Characterization of the Nanoporous Sucker Rings from Dosidicus gigas. *Adv. Mater.* **2009**, *21* (4), 401−406.
(3) Guerette, P. A.; Hoon, S.; Seow, Y.; Raida, M.; Masic, A.; Wong, F. T.; Ho, V. H.; Kong, K. W.; Demirel, M. C.; Pena-Francesch, A.; Amini, S.; Tay, G. Z.; Ding, D.; Miserez, A. Accelerating the design of biomimetic materials by integrating RNA-seq with proteomics and materials science. *Nat. Biotechnol.* **2013**, *31* (10), 908−915.
(4) Guerette, P. A.; Hoon, S.; Ding, D. W.; Amini, S.; Masic, A.; Ravi, V.; Venkatesh, B.; Weaver, J. C.; Miserez, A. Nanoconfined beta-Sheets Mechanically Reinforce the Supra-Biomolecular Network of Robust Squid Sucker Ring Teeth. *ACS Nano* **2014**, *8* (7), 7170−7179.
(5) Hiew, S. H.; Guerette, P. A.; Zvarec, O. J.; Phillips, M.; Zhou, F.; Su, H.; Pervushin, K.; Orner, B. P.; Miserez, A. Modular peptides from the thermoplastic squid sucker ring teeth form amyloid-like cross-β supramolecular networks. *Acta Biomater.* **2016**, *46*, 41−54.
(6) Hiew, S. H.; Miserez, A. Squid Sucker Ring Teeth: Multiscale Structure−Property Relationships, Sequencing, and Protein Engineering of a Thermoplastic Biopolymer. *ACS Biomater. Sci. Eng.* **2017**, *3* (5), 680−693.
(7) Adzhubei, A. A.; Sternberg, M. J.; Makarov, A. A. Polyproline-II helix in proteins: structure and function. *J. Mol. Biol.* **2013**, *425* (12), 2100−2132.
(8) Bochicchio, B.; Tamburro, A. M. Polyproline II structure in proteins: Identification by chiroptical spectroscopies, stability, and functions. *Chirality* **2002**, *14* (10), 782−792.
(9) Creamer, T. P.; Campbell, M. N. *Adv. Protein Chem.* **2002**, *62*, 263−282.
(10) Shi, Z. S.; Chen, K.; Liu, Z. G.; Ng, A.; Bracken, W. C.; Kallenbach, N. R. Polyproline II propensities from GGXGG peptides reveal an anticorrelation with beta-sheet scales. *Proc. Natl. Acad. Sci. U. S. A.* **2005**, *102* (50), 17964−17968.
(11) Shi, Z. S.; Olson, C. A.; Rose, G. D.; Baldwin, R. L.; Kallenbach, N. R. Polyproline II structure in a sequence of seven alanine residues. *Proc. Natl. Acad. Sci. U. S. A.* **2002**, *99* (14), 9190−9195.
(12) Van der Spoel, D.; Lindahl, E.; Hess, B.; Groenhof, G.; Mark, A. E.; Berendsen, H. J. C. GROMACS: Fast, flexible, and free. *J. Comput. Chem.* **2005**, *26* (16), 1701−1718.
(13) Bussi, G.; Donadio, D.; Parrinello, M. Canonical sampling through velocity rescaling. *J. Chem. Phys.* **2007**, *126* (1), 014101.
(14) Parrinello, M.; Rahman, A. Polymorphic Transitions in Single-Crystals - a New Molecular-Dynamics Method. *J. Appl. Phys.* **1981**, *52* (12), 7182−7190.
(15) Nose, S.; Klein, M. L. Constant Pressure Molecular-Dynamics for Molecular-Systems. *Mol. Phys.* **1983**, *50* (5), 1055−1076.
(16) Darden, T.; York, D.; Pedersen, L. Particle Mesh Ewald - an N.Log(N) Method for Ewald Sums in Large Systems. *J. Chem. Phys.* **1993**, *98* (12), 10089−10092.
(17) Jorgensen, W. L.; Chandrasekhar, J.; Madura, J. D.; Impey, R. W.; Klein, M. L. Comparison of Simple Potential Functions for Simulating Liquid Water. *J. Chem. Phys.* **1983**, *79* (2), 926−935.
(18) MacKerell, A. D.; Bashford, D.; Bellott, M.; Dunbrack, R. L.; Evanseck, J. D.; Field, M. J.; Fischer, S.; Gao, J.; Guo, H.; Ha, S.; Joseph-McCarthy, D.; Kuchnir, L.; Kuczera, K.; Lau, F. T. K.; Mattos, C.; Michnick, S.; Ngo, T.; Nguyen, D. T.; Prodhom, B.; Reiher, W. E.; Roux, B.; Schlenkrich, M.; Smith, J. C.; Stote, R.; Straub, J.; Watanabe, M.; Wiorkiewicz-Kuczera, J.; Yin, D.; Karplus, M. All-atom empirical potential for molecular modeling and dynamics studies of proteins. *J. Phys. Chem. B* **1998**, *102* (18), 3586−3616.
(19) Mackerell, A. D.; Feig, M.; Brooks, C. L. Extending the treatment of backbone energetics in protein force fields: Limitations of gas-phase quantum mechanics in reproducing protein conformational

DOI: 10.1021/acs.biomac.7b01280
Biomacromolecules 2017, 18, 4240−4248

distributions in molecular dynamics simulations. *J. Comput. Chem.* **2004**, *25* (11), 1400−1415.
(20) Sun, H. COMPASS: An ab Initio Force-Field Optimized for Condensed-Phase ApplicationsOverview with Details on Alkane and Benzene Compounds. *J. Phys. Chem. B* **1998**, *102* (38), 7338−7364.
(21) Lindon, J. C.; Tranter, G. E.; Koppenaal, D. *Encyclopedia of Spectroscopy and Spectrometry*; Elsevier Science, 2016.
(22) Micsonai, A.; Wien, F.; Kernya, L.; Lee, Y.-H.; Goto, Y.; Réfrégiers, M.; Kardos, J. Accurate secondary structure prediction and fold recognition for circular dichroism spectroscopy. *Proc. Natl. Acad. Sci. U. S. A.* **2015**, *112* (24), E3095−E3103.
(23) Bitan, G.; Kirkitadze, M. D.; Lomakin, A.; Vollers, S. S.; Benedek, G. B.; Teplow, D. B. Amyloid beta-protein (A beta) assembly: A beta 40 and A beta 42 oligomerize through distinct pathways. *Proc. Natl. Acad. Sci. U. S. A.* **2003**, *100* (1), 330−335.
(24) Bitan, G.; Fradinger, E. A.; Spring, S. M.; Teplow, D. B. Neurotoxic protein oligomers - what you see is not always what you get. *Amyloid* **2005**, *12* (2), 88−95.
(25) Streets, A. M.; Sourigues, Y.; Kopito, R. R.; Melki, R.; Quake, S. R. Simultaneous Measurement of Amyloid Fibril Formation by Dynamic Light Scattering and Fluorescence Reveals Complex Aggregation Kinetics. *PLoS One* **2013**, *8* (1), e54541.
(26) Mong, T. K. K.; Niu, A. Z.; Chow, H. F.; Wu, C.; Li, L.; Chen, R. *β*-Alanine-Based Dendritic *β*-Peptides: Dendrimers Possessing Unusually Strong Binding Ability Towards Protic Solvents and Their Self-Assembly into Nanoscale Aggregates through Hydrogen-Bond Interactions. *Chem. - Eur. J.* **2001**, *7* (3), 686−699.
(27) Copeland, R. A. *Enzymes: A Practical Introduction to Structure, Mechanism, and Data Analysis*; Wiley, 2004.
(28) Vatankhah-Varnoosfaderani, M.; GhavamiNejad, A.; Hashmi, S.; Stadler, F. J. Hydrogen Bonding in Aprotic Solvents, a New Strategy for Gelation of Bioinspired Catecholic Copolymers withN-Isopropylamide. *Macromol. Rapid Commun.* **2015**, *36* (5), 447−452.
(29) Khurana, R.; Uversky, V. N.; Nielsen, L.; Fink, A. L. Is Congo red an amyloid-specific dye? *J. Biol. Chem.* **2001**, *276* (25), 22715−22721.
(30) Latza, V.; Guerette, P. A.; Ding, D.; Amini, S.; Kumar, A.; Schmidt, I.; Keating, S.; Oxman, N.; Weaver, J. C.; Fratzl, P.; Miserez, A.; Masic, A. Multi-scale thermal stability of a hard thermoplastic protein-based material. *Nat. Commun.* **2015**, *6*, 8313.
(31) Barth, A.; Zscherp, C. What vibrations tell us about proteins. *Q. Rev. Biophys.* **2002**, *35* (4), 369−430.
(32) Zou, Y.; Li, Y.; Hao, W.; Hu, X.; Ma, G. Parallel *β*-Sheet Fibril and Antiparallel *β*-Sheet Oligomer: New Insights into Amyloid Formation of Hen Egg White Lysozyme under Heat and Acidic Condition from FTIR Spectroscopy. *J. Phys. Chem. B* **2013**, *117*, 4003−4013.
(33) Kajava, A. V.; Squire, J. M.; Parry, D. A. Beta-structures in fibrous proteins. *Adv. Protein Chem.* **2006**, *73*, 1−15.
(34) Hamley, I. W.; Dehsorkhi, A.; Castelletto, V.; Seitsonen, J.; Ruokolainen, J.; Iatrou, H. Self-assembly of a model amphiphilic oligopeptide incorporating an arginine headgroup. *Soft Matter* **2013**, *9* (19), 4794.
(35) Sunde, M.; Serpell, L. C.; Bartlam, M.; Fraser, P. E.; Pepys, M. B.; Blake, C. C. F. Common core structure of amyloid fibrils by synchrotron X-ray diffraction. *J. Mol. Biol.* **1997**, *273* (3), 729−739.
(36) Rathore, O.; Sogah, D. Y. Self-Assembly of *β*-Sheets into Nanostructures by Poly(alanine) Segments Incorporated in Multiblock Copolymers Inspired by Spider Silk. *J. Am. Chem. Soc.* **2001**, *123* (22), 5231−5239.
(37) Paramonov, S. E.; Jun, H.-W.; Hartgerink, J. D. Self-Assembly of Peptide−Amphiphile Nanofibers: The Roles of Hydrogen Bonding and Amphiphilic Packing. *J. Am. Chem. Soc.* **2006**, *128* (22), 7291−7298.
(38) Cui, H.; Webber, M. J.; Stupp, S. I. Self-assembly of peptide amphiphiles: From molecules to nanostructures to biomaterials. *Biopolymers* **2010**, *94* (1), 1−18.
(39) Versluis, F.; Marsden, H. R.; Kros, A. Power struggles in peptide-amphiphile nanostructures. *Chem. Soc. Rev.* **2010**, *39* (9), 3434.
(40) Dehsorkhi, A.; Castelletto, V.; Hamley, I. W. Self-assembling amphiphilic peptides. *J. Pept. Sci.* **2014**, *20* (7), 453−467.
(41) Hamley, I. W. Self-assembly of amphiphilic peptides. *Soft Matter* **2011**, *7* (9), 4122.
(42) Stupp, S. I.; Palmer, L. C. Supramolecular Chemistry and Self-Assembly in Organic Materials Design. *Chem. Mater.* **2014**, *26* (1), 507−518.
(43) Ortony, J. H.; Newcomb, C. J.; Matson, J. B.; Palmer, L. C.; Doan, P. E.; Hoffman, B. M.; Stupp, S. I. Internal dynamics of a supramolecular nanofibre. *Nat. Mater.* **2014**, *13* (8), 812−816.
(44) Hendricks, M. P.; Sato, K.; Palmer, L. C.; Stupp, S. I. Supramolecular Assembly of Peptide Amphiphiles. *Acc. Chem. Res.* **2017**, *50* (10), 2440−2448.

DOI: 10.1021/acs.biomac.7b01280
Biomacromolecules 2017, 18, 4240−4248